International Conference on Space Optics—ICSO 2006

Noordwijk, Netherlands

27–30 June 2006

Edited by Errico Armandillo, Josiane Costeraste, and Nikos Karafolas

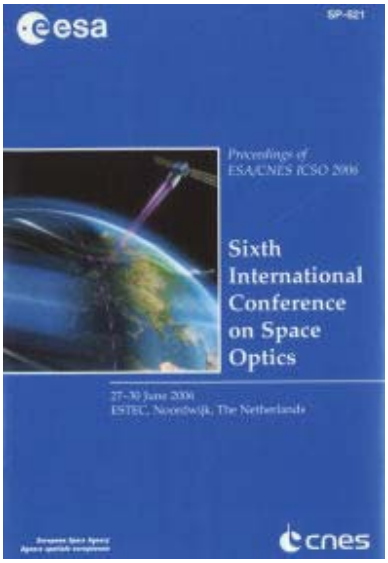

A microstructured wavefront filter for the DARWIN nulling interferometer

J. C. Flanagan, D. J. Richardson, M. J. Foster, I. Bakalski

International Conference on Space Optics — ICSO 2006, edited by Errico Armandillo, Josiane Costeraste, Nikos Karafolas, Proc. of SPIE Vol. 10567, 105672K · © 2006 ESA and CNES
CCC code: 0277-786X/17/$18 · doi: 10.1117/12.2308141

A MICROSTRUCTURED WAVEFRONT FILTER FOR THE DARWIN NULLING INTERFEROMETER

J. C. Flanagan[(1)], D. J. Richardson[(1)], M. J. Foster[(2)], I. Bakalski[(2)]

[(1)] Optoelectronics Research Centre, University of Southampton, SO17 1BJ, UK, Email: jcb@orc.soton.ac.uk
[(2)] Lidar Technologies Ltd, Arctic House, Rye Lane, Dunton Green, TN14 5HD, UK, Email: ibakalski@hovemere.com

ABSTRACT

The European Space Agency's space-based Darwin mission aims to directly detect extrasolar Earth-like planets using nulling interferometry. However, in order to accomplish this using current optical technology, the interferometer input beams must be filtered to remove local wavefront errors. Although short lengths of single-mode fibre are ideal wavefront filters, Darwin's operating wavelength range of 4 - 20 μm presents real challenges for optical fibre technology. In addition to the fact that step-index fibres only offer acceptable coupling efficiency over about one octave of optical bandwidth, very few suitable materials are transparent within this wavelength range. Microstructured optical fibres offer two unique properties that hold great promise for this application; they can be made from a single-material and offer endlessly single-mode guidance. Here we explore the advantages of using a microstructured fibre as a broadband wavefront filter for 4 - 20 μm.

1. INTRODUCTION

The discovery of an Earth-like body around a neighbouring star would have wide ranging significance to astronomy and, in particular, to the search for extra terrestrial life. Since the discovery of the first extrasolar planet in 1995 [1], more than 170 worlds have been detected in orbits around other main sequence stars. However, nearly all of these planets have been found via measurements of their parent star's radial velocity, a technique that intrinsically favours the detection of massive planets like Jupiter and Saturn. Other techniques, such as those utilizing photometric transits and gravitational microlensing, may be capable of detecting small terrestrial worlds, but are severely limited in application (transit data alone gives no information about a companion's mass, while microlensing events are, by their very nature, unpredictable and short lived [2]).

An alternative approach considered in the search for small terrestrial planets is direct detection via nulling interferometry, whereby the glare of the parent star is suppressed through the coherent combination of light collected by multiple telescopes [3, 4]. Spectroscopic characterization of light from a planet could also be used to provide clues as to the planets habitability. This is the goal of the European Space Agency's Darwin mission and NASA's Terrestrial Planet Finder (TFP), which aim to use space-based interferometers observing at wavelengths of 4 – 20 μm to directly detect extrasolar Earth-like planets and characterize them as possible abodes of life [5, 6]. The 4 – 20 μm observational window is defined by the scientific goal of detecting the spectral signatures of key biomarkers such as O_3, H_2O and CO_2, which are indicative of life. Observation at these wavelengths also aids detection as the brightness contrast between stars and planets falls by several orders of magnitude in the mid-infrared [3]. Even so, the requirements on the interferometer are stringent and to adequately detect an Earth-like world using current optical technology, the interferometer input beams must be 'filtered' to remove local wavefront errors [7 – 9].

Single-mode fibres form ideal wavefront filters as the output field profile is solely determined by the modal properties of the fibre. Such wavefront filters are typically referred to as *modal* filters. However, the observational wavelength range required by Darwin and the TFP presents significant challenges for optical fibre technology [10]. Since light can only be coupled into a step-index fibre (SIF) with acceptable efficiency over an optical bandwidth of about one octave, more than one fibre must be used. Currently, the accepted solution is to split the light from each telescope into 2 – 4 spectral windows that can each be addressed by individual fibres [9]. In addition, very few suitable materials are transparent within this wavelength range and finding thermally and chemically compatible core and cladding materials with a sufficiently low index contrast to ensure single-mode guidance is problematic. At present, the ability to fabricate fibres for transmission at wavelengths above 4 μm is a significant challenge in its own right.

One promising alternative for this type of application is microstructured optical fibre (MOF) technology, which allows endlessly single-mode structures to be created from materials with highly contrasting refractive indices, such as glass and air [11, 12]. This not only relaxes material requirements, permitting single-material waveguides, but also offers significant advantages for broadband single-mode applications [13, 14]. In this paper we investigate, via

Proc. '6th Internat. Conf. on Space Optics', ESTEC, Noordwijk, The Netherlands, 27-30 June 2006 (ESA SP-621, June 2006)

numerical calculations, the potential advantages that MOFs could offer relative to step-index designs for modal filtering over the wavelengths of 4 – 20 µm.

In the following sections, the principles of nulling interferometry and single-mode fibres as modal wavefront filters are briefly outlined. The basic properties of MOFs are then reviewed and the relative merits of step-index and microstructured fibres for use as a modal filter in Darwin / TFP-like applications over the wavelengths of 4 – 20 µm are explored.

2. NULLING INTERFEROMETRY

The challenges of directly detecting an Earth-like planetary system lie with the huge brightness contrast and tiny angular separation between a star and any orbiting planet. For example, if viewed from a distance of 4 parsecs, the brightness contrast between Earth and our Sun would be about 10^6 at best [3], with an angular separation of ~ 0.5 µrad. Nulling interferometry is one method that can be used to separate light arriving from slightly different directions and is particularly well suited to systems with high intensity contrast.

The simplest version of a nulling interferometer, known as a Bracewell interferometer, is used here to illustrate the basic principles of this technique. In the Bracewell configuration, shown in Fig. 3 [3], light from the star arrives at two identical telescopes simultaneously. Light from the planet, however, travels at a slight angle relative to the star-light and is thus collected by each telescope at slightly different times. By introducing a phase delay on the light from one of the telescopes and coherently combining both signals, an interference pattern is obtained. For a phase delay of $\lambda/2$, the star-light experiences destructive interference and by adjusting the baseline of the interferometer appropriately (i.e. for a telescope spacing of $\lambda_o/2\theta$), the light signal originating from the planet can be enhanced via constructive interference.

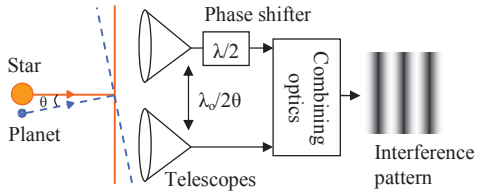

Fig. 1. Schematic of a Bracewell nulling interferometer.

3. MODAL WAVEFRONT FILTERS

The ratio between the interferometer output power at the regions of destructive and constructive interference determines the rejection ratio of the star-light relative to the light from the planet. In order to adequately detect the light of an Earth-sized world orbiting close enough to the star to be within the so-called 'life zone' [3], a rejection ratio of 10^5 – 10^6 is required [9]. The rejection ratio of a nulling interferometer is strongly degraded by wavefront errors and the above requirements correspond to instrumental tolerances that cannot be met with current optical technology.

However, these tolerances can be relaxed if a wavefront filter is used to eliminate the effect of local disturbances within the amplitude profile and the phase front of the input beams [7 – 9]. Single-mode waveguides are an attractive solution for this since their output field shape is essentially independent of the launch conditions, enabling correction of both the phase and amplitude profile [8]. Furthermore, single-mode fibres can efficiently correct wavefront defects with both high and low-order spatial frequencies, unlike simple pinholes [8]. The basic principles of a modal wavefront filter formed by a single-mode fibre are illustrated in Fig. 2.

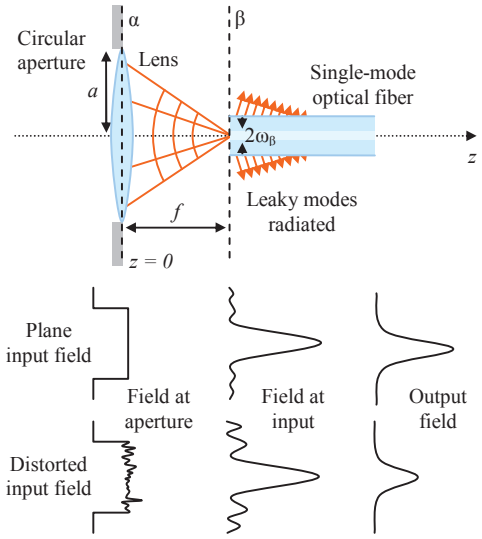

Fig. 2. Simple coupling arrangement and principles of a modal wavefront filter.

Here we assume a simple coupling arrangement where a freely propagating plane wave incident on a circular aperture of radius a is focused by a single thin, diffraction limited lens of focal length f located in the aperture plane α at $z = 0$. The fibre is placed at the focal point $z = f$ in the coupling plane β. In general, an infinite number of modes are excited at the coupling plane. However, all modes other than the fundamental mode (FM) are strongly attenuated and after a certain distance the majority of power is carried in the FM.

We note that this coupling arrangement is the simplest one could consider and that more complex systems may offer better broadband performance. However, using this scheme it is possible to present a clear comparison between the performance of MOFs, as calculated here, and the performance of SIF designs,

as reported elsewhere in the literature [10, 15]. Within this paper, results extracted from Fig. 3 in [10], which show the coupling efficiency as a function of the normalized frequency, are used for comparison.

The performance of a modal filter of a given length, *l*, is defined by the output power ratio between the FM and any other leaky higher-order, radiation or cladding modes excited at launch. This can be approximated by considering the output power ratio between the FM and the lowest-order leaky mode (corresponding to the LP_{11} mode below cut-off [10]); by assuming that all power not coupled into the FM is coupled into the lowest-order leaky mode (LM). The output power ratio in this 'worst case scenario' is thus defined as;

$$A = \frac{\eta 10^{\sigma}}{l(1-\eta)}, \text{ where } \sigma = l\alpha_{FM}/10 \ , \qquad (1)$$

α_{LM} is the leakage loss of the LM (in dB/m) and η is the fraction of power coupled into the FM at launch. By approximating the FM modal field of the fibre by a Gaussian of width ω_β (where ω_β is the width at which the intensity drops to $1/e^2$ of its peak value), and evaluating the coupling efficiency at the aperture plane, η can be written simply as [16]:

$$\eta(\lambda) = \frac{2}{\chi^2}\left(1 - e^{-\chi^2}\right)^2, \text{ where } \chi = \frac{a\pi\omega_\beta(\lambda)}{f\lambda} \qquad (2)$$

In this approximation, the maximum value of η is 0.81 and corresponds to χ = 1.121. Note that for the actual FM of a SIF, the maximum value of η is 0.786 and occurs for V = 2.405 [16]. The coupling system, with *a/f* as the sole free parameter, can only be optimized at a single wavelength (λ_{opt}), for which $a/f = 1.121\lambda_{opt}/(\pi\omega_\beta)$. For any given lens system, the broadband coupling efficiency is thus dependent on how ω_β evolves as a function of wavelength.

4. THE DARWIN MODAL FILTER

The work presented here was supported by the European Space Agency and focuses on the specific requirements of the Darwin mission, which include: (1) $A > 10^6$ (to ensure sufficient star-light rejection in the interferometer), and (2) a transmission loss (comprising both coupling and waveguide loss) of < 1.5 dB over the whole of the 4 – 20 μm observational window [9]. Since mid-infrared transmitting materials are relatively high loss and fragile in fibre form (compared to silica glass), it is desirable to use as short a fibre length as possible to minimize material losses and limit the amount of bending required. As such, an upper limit of approximately 50 cm for the modal filter length is defined in [9]. Note that for SIF designs, predictions indicate that it should be possible to achieve $A > 10^6$ in just a few cm of single-mode fibre [15]. However, experimental studies on chalcogenide and silver halide based SIFs designed for this application have shown that fibre lengths in the region of 20 – 50 cm are required in practice to obtain single-mode guidance [9].

5. MICROSTRUCTURED FIBRES

5.1 Introduction

One promising alternative for this type of application is microstructured optical fibre (MOF) technology, which has been shown to offer significant advantages in applications where broadband operation is required [13, 14]. Indeed, recent work has specifically highlighted the improved coupling efficiency of silica MOF technology for broadband interferometer applications at visible wavelengths [14]. MOF technology also significantly relaxes the requirements on suitable fibre materials; permitting wave-guiding structures to be created from a single material and enabling scale-invariant single-mode guidance in solid fibres made from two materials with highly contrasting refractive indices [11, 12]. MOFs have also been fabricated from a wide range of non-silica infrared transmitting materials including polycrystalline silver halide materials, which offer transmission across the entire 4 – 20 μm wavelength range [17, 18]. As such, MOFs offer real promise for broadband single-mode transmission at mid-infrared wavelengths.

However, the optical properties of MOFs are significantly different from SIFs and any comparison must be made carefully. In the following, the key differences between these two fibre types are discussed and the approach taken here to compare the two technologies for use as a modal filter in Darwin / TFP-like applications is outlined.

5.2 Microstructured fibres vs. step-index fibres

In a MOF, light is confined to the core by a cladding region with wavelength-scale structure. Most typically, the cladding consists of an array of small, longitudinal air holes in silica glass, and these fibres are known by many names, including (but not limited to) photonic crystal, holey, microstructured and photonic band-gap fibres. In this paper we consider only *index-guiding* solid core MOFs, as illustrated in Fig. 4. The defining parameters of this type of MOF are the hole-to-hole spacing (Λ), and the relative hole size (d/Λ).

The guidance mechanism of this type of MOF can be thought of as a modified form of total internal reflection, whereby the air holes lower the average or *effective* cladding index by an amount dependent on the fraction of light located within the air holes. As the wavelength (λ) increases, the light penetrates further into each air hole and the effective index (n_{eff}) of the MOF cladding regions falls, as illustrated in Fig. 5 (a),

where n_{core} is the core index and n_{clad} is the cladding index.

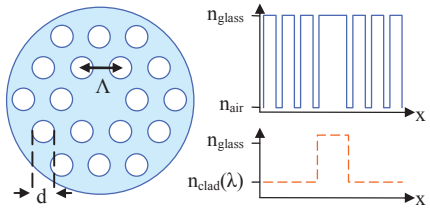

Fig.4. Defining parameters of index-guiding microstructured fibres.

The wavelength dependence of the cladding index in a MOF leads directly to a host of unique optical properties, including *endlessly* single-mode guidance. This phenomenon can be understood by considering the wavelength dependence of the V-parameter, where $V \propto (n_{core}^2 - n_{clad}^2)^{1/2}/\lambda$. A fibre is single-mode if V is below a certain critical value, which defines the single-mode (SM) cut-off. In a SIF, the cladding index is essentially constant (ignoring the effects of material dispersion) and the V-parameter of the fibre increases steadily towards short wavelengths, resulting in multi-mode guidance above a certain wavelength (λ_c), as illustrated in Figures 5 (b) and (c).

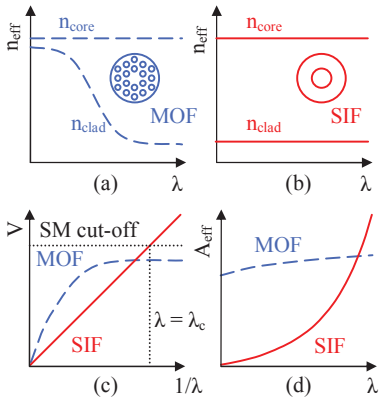

Fig.5. Schematic illustrations of the optical properties of MOFs (blue dashed line) and SIFs (red solid line) as a function of wavelength; (a) and (b) effective index, (c) V-parameter and (d) effective mode area.

In a MOF, the wavelength dependence of the cladding index counteracts the 1/λ dependence of the V-parameter, leading to an almost constant value of V in the short wavelength limit, as shown in Fig. 5 (c). If the air holes are small enough ($d/\Lambda \leq 0.4$ [19]), the absolute value of V can be low enough to ensure single-mode guidance at all wavelengths. The wavelength dependence of the cladding index in a MOF also leads to radically different behaviour in terms of the effective mode area (A_{eff}). In a SIF, the mode size expands dramatically towards long wavelengths, as the fibre becomes increasingly weakly guiding. However, due to the wavelength dependent cladding index, the A_{eff} of a MOF can be almost constant across a wide wavelength range, as illustrated in Fig. 5 (d) [20].

6. MICROSTRUCTURED FIBRE AS A MODAL FILTER

At first sight, the properties of MOFs, offering endlessly single-mode guidance and relatively constant mode area, seem ideal for broadband modal filtering applications. However, the inherently leaky nature of the MOF geometry must also be taken into consideration. In a MOF with a finite cladding, no true bound modes exist and every mode guided by the fibre (including the FM) has an associated leakage or *confinement* loss that increases towards long wavelengths [21]. As a result, the confinement loss of the FM (C_{FM}) must be taken into account when considering the overall transmission loss of the modal filter and also when determining its minimum length. Using the same assumptions as for Eq. (1), the minimum length of a MOF modal filter is defined as;

$$l_{min} = \frac{10\log_{10}\left(A[1-\eta]/\eta\right)}{\Delta C}, \quad \text{where } \Delta C = C_{FM} - C_{LM} \qquad (3)$$

and C_{LM} is the confinement loss of the next lowest loss mode after the FM. The second lowest loss mode of a MOF (once again denoted LM for "leaky-mode") is an LP_{11}-like mode, as illustrated in Figs 6 (b) and (c) [19]. Since ΔC increases towards long wavelengths, l_{min} is thus defined at the shortest operating wavelength, which corresponds to 4 µm for the case considered here. The modal fields and associated confinement losses of each MOF considered here are calculated using commercially available software based on the finite element method, using anisotropic perfectly matched absorbing boundary layers [22]. The confinement losses are extracted directly from the imaginary part of the propagation constant. In all calculations presented here we have assumed a single material fibre with a material index of 2.167, which corresponds to the polycrystalline material silver bromide at 10 µm [23]. However, since many infrared transmitting materials have similar values of refractive index [23], the results presented here are generally applicable to a wider range of suitable materials. The effects of material dispersion have not been considered. Example intensity profiles of the first three modes of a MOF with $\Lambda = 20$ µm, $d/\Lambda = 0.4$ and three rings of air holes are shown in Fig. 6 for a wavelength of 4 µm.

In all calculations of η presented here, the FM of each MOF considered is approximated by a Gaussian with $A_{eff} = \pi\omega_\beta^2$, where A_{eff} is evaluated from the modal field calculated using the finite element technique mentioned above, using the definition in

[24]. Although the modal field of a MOF is slightly hexagonal in form (as shown in Fig. 3 (a)), the field shape can be well approximated by a Gaussian function. For the MOF designs considered here, the overlap between the fundamental mode and a Gaussian of optimal width is typically ~ 97 % over the whole 4 – 20 μm spectral range.

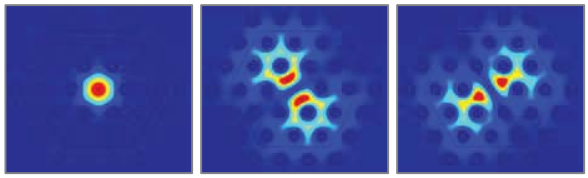

Fig.6. Calculated modal intensity profiles for Λ = 20 μm, d/Λ = 0.4, N =3. (a) Fundamental mode, C_{FM} = 0.002 dB/m (b) and (c) First two higher-order modes, C_{LM} = 150 dB/m. Open circles indicate hole positions. (Large open hexagon defines a region of higher density mesh used in the calculations).

7. RESULTS

In the MOF geometry considered here (illustrated in Fig. 4), there are three free parameters; the hole spacing (Λ), the hole size (d) and the number of rings of holes (N). Assuming the FM is reasonably well confined to the core region, the optimal coupling efficiency at a given wavelength depends solely on Λ and d. However, the *broadband* coupling efficiency is also dependent on the wavelength at which the coupling system is optimized (λ_{opt}), which itself has a different optimal value for each fibre geometry considered. In addition, the confinement loss of the FM and the minimum filter length are interlinked quantities that depend on all three fibre parameters (Λ, d and N). As such, the evaluation of a MOF structure for optimal filter performance over the whole operating wavelength range is not a trivial task.

To simplify matters, we look first at defining a single parameter that can be used to gauge the average coupling efficiency over the 4 – 20 μm wavelength range for a single MOF structure, independent of λ_{opt}. As mentioned above, the broadband coupling efficiency for the assumed coupling system is determined solely by $\omega_\beta(\lambda)$. From Eq. (1) it can be seen that η will be constant with respect to wavelength if $\omega_\beta \propto \lambda$; i.e. if $A_{eff} \propto \lambda^2$. Fibre parameters that lead to high average values of η can thus be gauged by assessing the relative change in A_{eff}/λ^2 over the relevant wavelength range. The relative change in A_{eff}/λ^2 between the wavelengths of λ_1 and λ_2, where $\lambda_1 < \lambda_2$, is evaluated here as;

$$Q = \frac{1}{P}\int_{\lambda_1}^{\lambda_2} A_{eff}/\lambda^2 d\lambda \ , \ \text{where} \ P = (A_{eff}/\lambda^2)_{\lambda=\lambda_2} \quad (4)$$

In this definition, low values of Q thus correspond to high average values of η. Values of Q calculated from predicted values of $A_{eff}/P\lambda^2$ are plotted in Fig. 7 for MOF structures in the range 9 μm < Λ < 21 μm and 0.18 < d/Λ < 0.45. This plot demonstrates that low values of Q can be achieved with small values of Λ and d/Λ.

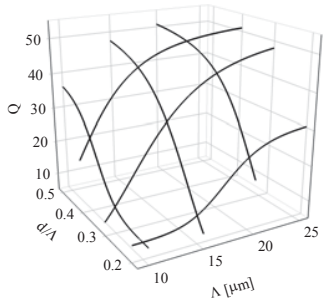

Fig.7. The parameter Q plotted as a function of Λ and d/Λ.

Although the parameter Q is a very simple way of quantifying the broadband coupling efficiency, we find that it works well for the range of fibre structures considered here. To illustrate this, the coupling loss (ξ = -10log10[η]) for six different MOFs are plotted in Figs 8 (a) – (f), respectively. Values of Λ, d/Λ and Q are indicated on each plot. Results correspond to three different lens systems, optimized at λ = 6.0, 8.0 and 10.0 μm, which are representative of the best-case for each fibre considered. The typical coupling loss for a SIF with λ_c = 4.0 μm is shown for comparison in Fig. 8 (g) for three different lens systems, optimized at V = 2.4, 1.2 and 1.0 (where $V_{opt} \propto 1/\lambda_{opt}$) [3]. These examples not only demonstrate that the parameter Q is a good measure of the average coupling performance, but also show that the MOF geometry can be tailored to offer significantly improved broadband coupling efficiency relative to a SIF that is single-mode over the entire 4 – 20 μm window.

However, the practicalities of fabrication restrict any MOF design to a relatively modest number of holes and we must therefore consider the confinement losses of the FM (C_{FM}) for structures that are practical to fabricate. Whilst the fabrication techniques for silica-based MOFs are fairly mature (a selection of designs have been commercially available for several years), the technology for fabricating fibres from infrared transmitting non-silica glasses is far less established for both SIFs and MOFs. Currently, the vast majority of single-material MOFs made from non-silica glasses are simple structures comprising just three large air holes [25], although solid MOFs fabricated from two non-silica materials with up to 5 rings of low-index inclusions have been reported [26]. Here we choose to consider N = 7 as the upper limit that is practically feasible to fabricate in materials suitable for the 4 – 20 μm wavelength range. The maximum tolerable value of C_{FM} is defined here as a 1 dB loss over the minimum length, which is comparable

with the lowest possible loss for the coupling system assumed here (see Fig. 2 and associated text). Since confinement losses increase towards long wavelengths, we need only consider C_{FM} at the longest operating wavelength.

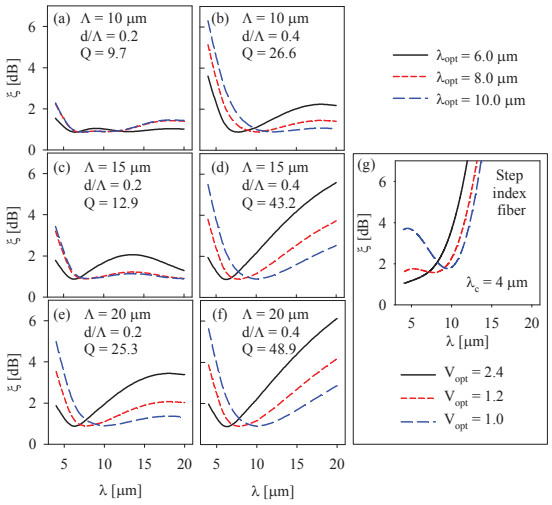

Fig. 8. (a) – (f) Coupling loss as a function of wavelength for different MOFs. Values of Λ, d/Λ, Q and λ_{opt} are indicated on each plot. (g) Coupling loss as a function of wavelength for a SIF with λ_c = 4 μm, extracted from results in Fig 3 in [10]. $V_{opt} \propto 1/\lambda_{opt}$.

In addition, the process of determining an appropriate MOF structure is not merely a case of sufficiently increasing N in order to reduce C_{FM} to practical levels. Increasing N also lowers C_{LM} (such that ΔC decreases), and the minimum fibre length required to achieve a certain value of A thus increases with the addition of each ring of air holes. As such, there is a trade-off between lowering C_{FM} and minimizing the transmission losses that result from material attenuation. This argument also applies equally to the fibre parameters Λ and d/Λ; minimizing the required filter length requires a leaky structure (achieved via small values of Λ, d/Λ), whilst maintaining practically low values of C_{FM} requires the exact opposite (i.e. large values of Λ, d/Λ). To determine the optimal MOF structure for a modal filter it is thus necessary to look at the trade-off between material attenuation (defined by l_{min}, which is determined at λ = 4 μm) and C_{FM} (which is largest at λ = 20 μm), as a function of Λ, d/Λ and N. At the same time, we must also consider the contribution from coupling loss.

The graphs in Fig. 9 illustrate the relationships between the three fibre parameters (Λ, d/Λ and N) and the three key filter properties (C_{FM}, l_{min} and Q) as a function of N for Λ = 10, 15 and 20 μm and d/Λ = 0.2, 0.3 and 0.4. Figures 9 (a) – (c) show C_{FM} at λ = 20 μm for $l = l_{min}$ and the corresponding values of l_{min} are shown in Figures 8 (d) – (e). The grey horizontal lines indicate the upper limits defined previously for C_{FM} and l_{min}. Values of Q are indicated by each curve. All results correspond to a lens system optimized at λ = 8 μm, which is representative of the best-case for each fibre considered. These results illustrate the direct trade-offs between achieving low values of Q and C_{FM} with a minimum number of air holes in as short a length as possible and highlight those MOF designs that are practically useful. Note that values of d/Λ > 0.4, were not considered in any detail as the minimum length required dramatically increases due to the onset of well confined higher-order modes. For example, we find that for Λ = 10 μm and d/Λ = 0.5, the minimum fibre length is in excess of 10 m.

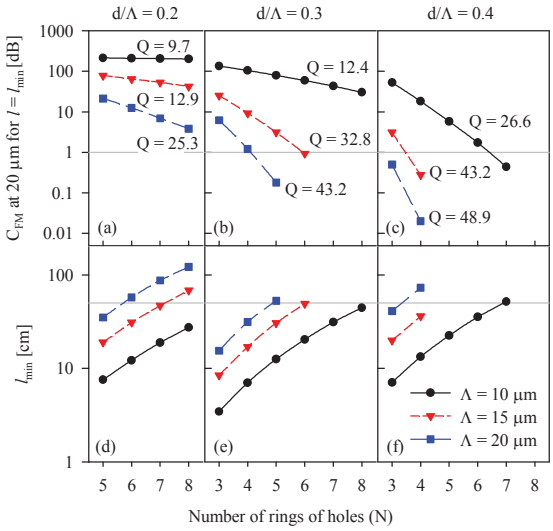

Fig. 9. (a) – (c) C_{FM} for $l = l_{min}$ at λ = 20 μm as a function of N for Λ = 10, 15 and 20 μm. The corresponding minimum length, l_{min}, (for which $A = 10^6$ at λ = 4 μm) is shown in (d) – (f). In (a) and (d) d/Λ = 0.2, in (b) and (e) d/Λ = 0.3, and in (c) and (f) d/Λ = 0.4. λ_{opt} = 8 μm.

By looking at Fig. 9, it is possible to determine values of Λ and d/Λ that result in acceptable filter performance for a feasibly low value of N. For example, although a MOF with Λ = 10 μm and d/Λ = 0.2 has excellent broadband coupling efficiency, it is not possible to adequately confine the FM with a reasonable number of air holes in this case. More detailed results for this fibre, plotted in Fig. 10, clearly illustrate this fact. The coupling loss is shown in Fig. 10 (a) and the transmission loss (ξ_T), comprising both the coupling and confinement loss over the minimum length ($l_{min}C_{FM}$), is shown in Fig. 10 (b). This demonstrates that the fibre transmission is completely overwhelmed by confinement loss for λ > 11 μm. Furthermore, the minimum length of fibre required in this example is ~ 20 cm, which is an order of magnitude greater than that required (in principle) for a SIF modal filter [15]. Consequently, despite the excellent coupling efficiency, the overall performance of this MOF is worse than that predicted for a SIF.

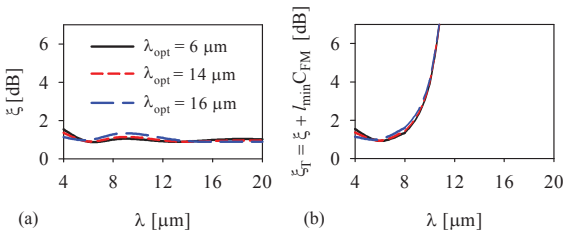

Fig.10. Λ = 10 μm, d/Λ = 0.2, N = 7 (a) Coupling loss as a function of wavelength (b) Transmission loss as a function of wavelength for $l = l_{min}$. All results shown for three representative values of λ_{opt}.

However, if the hole size is increased to d/Λ = 0.4, we see that the FM can be well confined with as few as 7 rings of air holes with l_{min} ~ 50 cm for Λ = 10 μm, as shown in Figs 9 (c) and (f). Whilst the coupling losses are higher than for the previously highlighted example (see Fig. 8 (a) and (b)), the C_{FM} is significantly lower, resulting in good overall performance. The transmission loss of this MOF is plotted in Fig. 11 (a) for three representative values of λ_{opt}. This is obviously a significant improvement compared with a SIF that is single-mode at all wavelengths within the 4 – 20 μm range, as shown in Fig. 11 (b). However, this does not necessarily represent a fair comparison since it is possible to lower ξ over a broader wavelength range in a SIF by increasing λ_c. As examples, Figures 11 (c) and (d) show ξ_T for SIFs with λ_c = 6.6 and 8.4 μm for three representative values of V_{opt}. Comparing the results in this way, we see that the MOF geometry does indeed offer lower loss transmission over a broader wavelength range than a SIF. For example, for ξ_T < 2 dB, a MOF based modal filter can offer transmission over λ ~ 6.3 – 20 μm, whilst a SIF version only offers transmission over λ ~ 8.4 – 20 μm (for V_{opt} = 1.2 in Fig. 11 (d)). Furthermore, while a MOF design enables transmission over the whole 4 – 20 μm range for ξ_T < 3.7 dB, this can only be achieved for λ ~ 6.6 – 20 μm, at best in a SIF (for V_{opt} = 1.0 in Fig. 11 (c)).

Once again, the minimum length required by this MOF (~ 50 cm) is substantially longer than that predicted for a SIF based modal filter (few cm). However, SIFs made from silver halide materials have been reported with transmission losses < 1 dB/m over the 4 – 20 μm wavelength range [18]. Assuming that similar values can be achieved in a MOF geometry, a length of 50 cm would incur an additional 0.5 dB of loss, at most. Even with this taken into consideration, the overall performance of a MOF based modal filter still represents an improvement over the capabilities of SIF technology. Furthermore, as noted in Section 4, experimental work on SIFs developed for this application has shown that ~ 20 – 50 cm lengths of fibre are required in practice to obtain single-mode operation [9]. Whilst reports do not indicate why the lengths of SIF required for single-mode operation are longer in practice than predicted, it is worth noting that silica MOFs are typically observed to be single-mode in shorter lengths than predictions specify [27, 28].

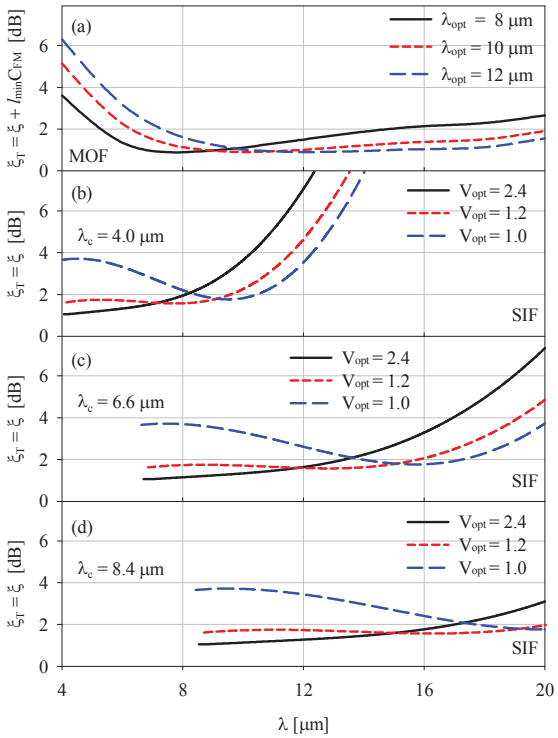

Fig.11. (a) Transmission loss as a function of wavelength for a MOF with Λ = 10 μm, d/Λ = 0.4, N = 7. (b), (c) and (d) Coupling loss as a function of wavelength for SIFs with λ_c = 4.0, 6.6 and 8.4 μm respectively (adapted from Fig. 3 in [10]). $V_{opt} \propto 1/\lambda_{opt}$.

8. DISCUSSION AND CONCLUSION

Within this paper, we have explored the advantages of using a single-mode microstructured optical fibre (MOF) as a broadband modal filter in the Darwin nulling interferometer, operating between the wavelengths of 4 – 20 μm. This spectral range presents significant challenges for optical fibre technology, not least because very few suitable materials are transparent at these wavelengths, but also because the coupling efficiency falls dramatically at wavelengths more than an octave above the single-mode cut-off in step-index fibre (SIF) designs [9]. MOFs offer two unique properties that hold great promise for this application; they can be made from a single-material (or from two materials with highly contrasting refractive indices) and offer endlessly single-mode guidance [11, 12]. However, since the properties of MOFs are significantly different from SIFs, any comparison must be made carefully. By considering structures that are practical to fabricate, and accounting for the overall performance, we have shown that a MOF modal filter can indeed offer lower loss transmission over a broader wavelength range than can be achieved with a SIF based design.

Nevertheless, it should be appreciated that the work presented here is only a first step towards developing an optimised modal filter, a process that should obviously include the design of the coupling optics in parallel. The results shown here demonstrate that the optical properties of MOFs can be tailored via the fibre geometry to improve performance, but we have only considered variations to the most basic MOF parameters: the number of air holes and their size and spacing. The MOF geometry offers many more degrees of design freedom in addition to these basic parameters; for example, a graded index fibre profile can be created simply by grading the size of the air holes. The ability to further optimise the optical performance in this way thus offers a potentially powerful route towards a tailor-made solution for the Darwin modal filter.

9. REFERENCES

1. M. Mayor and D. Queloz, "A Jupiter-mass companion to a solar-type star," Nature **378**, 355 – 359 (1995).
2. N. Woolf and J. R. Angel, "Astronomical searches for earth-like planets and signs of life," Astron. Astrophys. **36**, 507-537 (1998).
3. R.N. Bracewell, "Detecting nonsolar planets by spinning infrared interferometer," Nature **274**, 780 – 781 (1978).
4. J.R.P. Angel, A.Y.S. Cheng and N.J. Woolf, "A space telescope for infrared spectroscopy of Earth-like planets," Nature **322**, 341 – 434 (1978).
5. C.V.M. Fridlund, "Darwin – The Infrared Space Interferometry Mission," ESA bulletin, **103**, 20 – 25 (2000). http://planetquest.jpl.nasa.gov/Navigator/library/tpfI414.pdf
7. M. Ollivier and J. Mariotti, "Improvement in the rejection rate of a nulling interferometer by spatial filtering," Appl. Opt. **36**, 5340 – 5346 (1997).
8. B. Mennesson, M. Ollivier and C. Ruilier, "Use of single-mode waveguides to correct the optical defects of a nulling interferometer," J. Opt. Soc. Am. A **19**, 596 – 602 (2002).
9. Darwin Payload Definition Document SCI-A/2005/301/ Darwin/DMS/LdA
10. O. Wallner, W.R. Leeb and R. Flatscher, "Design of spatial and modal filters for nulling interferometry", Proc. SPIE **838**, 668-679 (2003).
11. P. St. J. Russell, "Photonic crystal fibers," Science **299**, 358 - 362, (2003).
12. J.C. Knight, "Photonic crystal fibres," Nature **424**, 847 - 851, (2003).
13. J.C. Baggett, T.M. Monro, D.J. Richardson, "Mode area limits in practical single-mode fibers," CMD6 CLEO'05, Baltimore, USA, 22-27th May 2005.
14. J.C. Corbett and J.R. Allington-Smith, "Coupling starlight into single-mode photonic crystal fiber using a field lens," Opt. Express **13**, 6527-6540 (2005)
15. O. Wallner, W.R. Leeb, and P.J. Winzer "Minimum Length of a Single-mode Spatial Filter" J. Opt. Soc. Am. A. **19** 2445 – 2448 (2002).
16. O. Wallner, P.J. Winzer and W.R. Leeb, 'Alignment tolerances for plane wave to single-mode fiber coupling and their mitigation by use of pigtailed collimators,' Appl. Opt. **41** 637 – 643 (2001).
17. E. Eran Rave, P. Ephrat, M. Goldberg, E. Kedmi, and A. Katzir, 'Silver Halide Photonic Crystal Fibers for the Middle Infrared,' Appl. Opt. **43**, 2236 - 2241 (2004).
18. L.N. Butvina, E. M. Dianov, N. V. Lichkova, V. N. Zavgorodnev, L. Kuepper, "Crystalline silver halide fibers with optical losses lower than 50 dB/km in broad IR region and their applications", Proceedings of SPIE **4083** (2000).
19. G. Renversez, F. Bordas, and B.T. Kuhlmey, "Second mode transition in microstructured optical fibers: determination of the critical geometrical parameter and study of the matrix refractive index and effects of cladding size," Opt. Lett. **30**, 1264-1266 (2005).
20. N.A. Mortensen, "Effective area of photonic crystal fibers," Opt. Express **10**, 341-348 (2002).
21. T.P. White, R.C. McPhedran, C.M. de Sterke, L.C. Botten, M. J. Steel, 'Confinement losses in microstructured optical fibers,' Opt. Lett. **26**, 1660 – 1662 (2001).
22. http://www.comsol.com/products/electro/
23. http://www.crystran.co.uk/products.asp
24. Govind P. Agrawal, Nonlinear Fiber Optics, 3rd Ed p44, (Academic Press 2001).
25. T.M. Monro, H. Ebendorff-Heidepriem, X. Feng, "Non-silica microstructured optical fibers", Ceramic Transactions, **163**, 29-48 (2005).
26. F. Luan, A. K. George, T. D. Hedley, G. J. Pearce, D. M. Bird, J. C. Knight, and P. S. J. Russell, "All-solid photonic bandgap fiber," Opt. Lett. **29**, 2369-2371 (2004).
27. H.P. Uranus, H.J.W.M. Hoekstra, and E. van Groesen, "Modes of an endlessly single-mode photonic crystal fiber: a finite element investigation," Proc. IEEE/LEOS Benelux Chapter, 2004, Ghent.
28. A. Argyros and I.M. Bassett, "Counting Modes in Optical Fibres with Leaky Modes," Symposium on Optical Fiber Measurements, September 24-26, Boulder, Colorado, USA. pp. 135-138.

ACKNOWLEDGEMENTS

This work was supported by the European Space Agency under ESTEC Contract 18609/04/NL/PM, '*Photonic Crystal (Holey) Fibres for Space Applications*'. The authors wish to thank Nicholas Bantin, (Lidar Technologies Ltd, UK), Iain McKenzie (ESTEC, ESA, The Netherlands), Xian Feng and Ravi Vinnakota (ORC, UK) and Oswald Wallner (Vienna University of Technology, Austria) for valuable advice and discussions.